Antarct. Meteorite Res., **15**, 97–113, 2002

Cosmic-ray exposure age and heliocentric distance of the parent body of H chondrites Yamato-75029 and Tsukuba

Daisuke Nakashima[1], Tomoki Nakamura[2], Minoru Sekiya[2] and Nobuo Takaoka[2]

[1]*Department of Earth and Planetary Sciences, Graduate School of Sciences, Kyushu University 33, Hakozaki, Fukuoka 812-8581*
[2]*Department of Earth and Planetary Sciences, Faculty of Sciences, Kyushu University 33, Hakozaki, Fukuoka 812-8581*

Abstract: Many small pieces of the H chondrites Yamato (Y-) 75029 and Tsukuba were investigated to characterize signatures of light noble gases. These meteorites contain large amounts of solar gases as well as cosmogenic ones. A simple regolith exposure model was developed in order to explain the correlations among solar ^{20}Ne and ^{36}Ar and cosmogenic ^{21}Ne concentrations. Based on the regolith model, the parent body exposure ages, heliocentric distances, and space exposure ages of the two meteorites were calculated. The parent body exposure ages were more than 5.5 Ma and 11.8 Ma for Y-75029 and Tsukuba, respectively. The heliocentric distances were $2.2\pm^{0.3}_{0.6}$ AU and $4.2\pm^{0.4}_{1.2}$ AU for Y-75029 and Tsukuba, respectively. The space exposure age of Y-75029 was 5.2–5.8 Ma, whereas that of Tsukuba was 8.1 ± 0.6 Ma.

It has been suggested that the parent bodies of H chondrites are S-type asteroids with orbits that range from 2 to 3.5 AU in the present solar system. On the other hand, the obtained heliocentric distances of Y-75029 and Tsukuba indicate locations of the parent bodies in the past when some parts of the meteorites were exposed to the sun. The heliocentric distance for Y-75029 is in a good agreement with current S-type asteroid distribution, while that for Tsukuba is at the upper tail of the distribution.

1. Introduction

Where were the meteorite parent bodies in the solar system? Important clues can be found in gas-rich brecciated meteorites that show characteristic dark and light structure. The dark portions contain both solar and cosmogenic noble gases (Suess *et al.*, 1964; Signer, 1964) indicative of direct exposure to the sun, whereas the light portions contain only cosmogenic ones, indicating some shielding to the solar radiation. It is generally agreed that these brecciated meteorites originated from the surface regoliths of parent-body asteroids (Wänke, 1965; Wilkening, 1971; Pellas, 1972; Schultz *et al.*, 1972; Rajan, 1974; Anders, 1975; Housen *et al.*, 1979; Keil, 1982).

The fluxes of solar winds (SW) and solar energetic particles (SEP), which were implanted directly on the surface of the meteorite parent body, are inversely related to the square of the heliocentric distance of the meteorite parent body. Galactic cosmic rays (GCR), which produce spallogenic nuclides in the meteorite parent body and meteoroids, have a constant flux throughout the whole solar system. Applying this energetic particle environment to locate meteorite parent bodies in the solar system, Anders (1975) calculated the heliocentric distances of some meteorite parent bodies on the basis of the noble gas data. Wieler *et al.* (1989) calculated a parent body exposure age of more than 20 Ma and a 2–3 AU for the heliocentric distance of the H chondrite Fayetteville.

The purpose of this study is to determine the parent body exposure ages and heliocentric distances of two H chondrites, Y-75029 and Tsukuba, in order to understand the orbit and regolith evolution of H chondrite parent bodies. The two meteorites are known to contain solar and cosmogenic gases (Takaoka *et al.*, 1981; Okazaki *et al.*, 1998). Concentrations of solar ^{20}Ne and ^{36}Ar and cosmogenic ^{21}Ne in many pieces of the meteorites were determined by noble gas analysis, and the parent body exposure ages, heliocentric distances, and space exposure ages of the two meteorites were calculated.

2. Experimental procedures

2.1. Samples and petrologic types

Before noble gas analysis, we sliced the meteorite chips using a diamond-bearing wheel cutter and observed the rough surfaces of the slices with a stereoscope. Y-75029 is dark brownish color due to terrestrial weathering of the metallic portions and as a result the dark-light structure can not be recognized in this meteorite. On the other hand, the dark-light structure is clearly observed in Tsukuba. The darkening is caused by the existence of tiny iron particles on the surface of grains (Keller and McKay, 1997). It was suggested that the iron particles are produced by the reduction of FeO in silicate minerals as a result of micrometeorite impacts (Sasaki *et al.*, 2001). After observation with a stereoscope, Y-75029 and Tsukuba sample slices were polished for observation by electron microscopy. The dark-light structure is not visible in Tsukuba after polishing. Probably this is because the darkened mineral surfaces were polished away and light-colored mineral interiors are coming out, which blurred the boundary between the dark and light portions.

The chemical compositions of the olivine and pyroxene in Y-75029 and Tsukuba were analyzed with an electron probe microanalyzer (EPMA: JEOL JXA-733 superprobe) equipped with a wave-length-dispersive X-ray spectrometer (WDS). WDS quantitative analyses were performed at 15 kV accelerating voltage and 10 nA beam current with a focused beam 2 μm in diameter. Natural minerals such as diopside and olivine were used for standardization. Quantitative chemical compositions were obtained *via* the ZAF correction method. The detection limit is 0.05 wt% for the elements analyzed and the reproducibility is less than $\pm 5\%$ of the concentrations of each element based on the repeated analysis of the standard minerals.

The petrologic types of Y-75029 and Tsukuba were determined from the dispersion of olivine and pyroxene chemical compositions, using the criteria of Van Schmus and Wood (1967). Y-75029 is assigned a petrologic type of 3 to 4, in agreement with the analyses of Yanai and Kojima (1987). In contrast, the petrologic type of Tsukuba is greater than 5, compatible with the classification of Grossman (1996).

2.2. Noble gas analysis

Meteorite samples were crushed into small pieces for noble gas analysis in order to separate noble gas-rich and -poor portions. As we mentioned before, the dark-light structure is not observed in Y-75029. Therefore, Y-75029 was only crushed into one group of small pieces. On the other hand, Tsukuba exhibits the dark-light structure and was separated into the dark and light portions. Each portion was then crushed into smaller pieces weighing 0.7 to 37.1 mg. We analyzed 23 pieces of Y-75029 and 30 pieces of Tsukuba. Each sample was heated at 1700°C to extract the noble gases. The concentrations and isotopic ratios of He, Ne, and Ar were measured using a noble gas mass spectrometer at Kyushu University (Nakamura and Takaoka, 2000). Solar and cosmogenic components were separated on the basis of Ne and Ar isotopic ratios. The equations used to obtain the concentrations of solar ^{20}Ne ($^{20}Ne_S$) and ^{36}Ar ($^{36}Ar_S$) and cosmogenic ^{21}Ne ($^{21}Ne_C$) are:

$$^{20}\mathrm{Ne_S} = {}^{22}\mathrm{Ne} \times \frac{(^{21}\mathrm{Ne}/^{22}\mathrm{Ne}) - (^{21}\mathrm{Ne}/^{22}\mathrm{Ne})_C}{(^{21}\mathrm{Ne}/^{22}\mathrm{Ne})_S - (^{21}\mathrm{Ne}/^{22}\mathrm{Ne})_C} \times (^{20}\mathrm{Ne}/^{22}\mathrm{Ne})_S, \tag{1}$$

$$^{21}\mathrm{Ne_C} = {}^{22}\mathrm{Ne} \times \frac{(^{21}\mathrm{Ne}/^{22}\mathrm{Ne})_S - (^{21}\mathrm{Ne}/^{22}\mathrm{Ne})}{(^{21}\mathrm{Ne}/^{22}\mathrm{Ne})_S - (^{21}\mathrm{Ne}/^{22}\mathrm{Ne})_C} \times (^{21}\mathrm{Ne}/^{22}\mathrm{Ne})_C, \tag{2}$$

$$^{36}\mathrm{Ar_S} = {}^{36}\mathrm{Ar} \times \frac{(^{38}\mathrm{Ar}/^{36}\mathrm{Ar})_C - (^{38}\mathrm{Ar}/^{36}\mathrm{Ar})}{(^{38}\mathrm{Ar}/^{36}\mathrm{Ar})_C - (^{38}\mathrm{Ar}/^{36}\mathrm{Ar})_S}, \tag{3}$$

where $(^{21}Ne/^{22}Ne)_C$ is the x-coordinate of the point at which the correlation line of measured data and the line $(^{20}Ne/^{22}Ne)_C = 0.8$ (Eugster, 1988) intersect in the Ne three-isotope-diagram (Fig. 1) (see Eugster, 1988), and $(^{20}Ne/^{22}Ne)_S$ is the y-coordinate of the intersection between two straight lines in Fig. 1. The first line is the correlation line of measured data, and the second line is the tie line connecting the components SW-Ne and SEP-Ne (Benkert *et al*., 1993); $(^{20}Ne/^{22}Ne, ^{21}Ne/^{22}Ne)_{SW} = (13.8, 0.0328)$, $(^{20}Ne/^{22}Ne, ^{21}Ne/^{22}Ne)_{SEP} = (11.2, 0.0295)$. The isotopic ratios of cosmogenic-Ne $(^{20}Ne/^{22}Ne, ^{21}Ne/^{22}Ne)_C$ are $(0.8, 0.806)_{Y\text{-}75029}$, $(0.8, 0.864)_{Tsukuba}$. $(^{38}Ar/^{36}Ar)_C$ was calculated from the production rate data of $^{36}Ar_C$ and $^{38}Ar_C$ given by Leya *et al.* (2000) and the chemical compositions of Y-75029 (Haramura *et al*., 1983) and Tsukuba (Jarosewich, 1990; the average chemical composition of H chondrites is applied for Tsukuba). $(^{38}Ar/^{36}Ar)_S$ is obtained from the ordinate intercept method applied to the diagram of $^{38}Ar/^{36}Ar$ *vs.* $1/^{36}Ar$ (Fig. 2). $(^{38}Ar/^{36}Ar)_S$ is the mixture of SW-Ar (0.182, Benkert *et al*., 1993) and SEP-Ar (0.205, Benkert *et al*., 1993). This method for $(^{38}Ar/^{36}Ar)_S$ determination follows Eugster *et al.* (1996). Solar-Ar of $(^{38}Ar/^{36}Ar)_S = 0.189$ and 0.186 were obtained for Y-75029 and Tsukuba, respectively.

3. Results of noble gas analysis

Results of noble gas analyses of Y-75029 and Tsukuba are shown in Tables 1 and 2, where on the basis of $^{20}Ne/^{22}Ne$, we separated samples into solar-gas-rich and solar-gas-poor portions. The samples with $^{20}Ne/^{22}Ne$ of more than 10 are assigned to solar-gas-rich portions, while the others are considered to be solar-gas-poor portions. Samples of the dark portions of Tsukuba tend to contain large amounts of solar and cosmogenic noble gases, whereas samples of the light portions contain only cosmogenic gases. However, some of the dark samples contain only cosmogenic gases, while some of the light samples contain small amounts of solar gases. This may indicate that the separation of dark and light portions from bulk samples was imperfect.

Figure 1 shows a Ne three-isotope-diagram. The Ne isotopic ratios are distributed on a tie line between solar-Ne and cosmogenic-Ne, showing that Ne in the individual

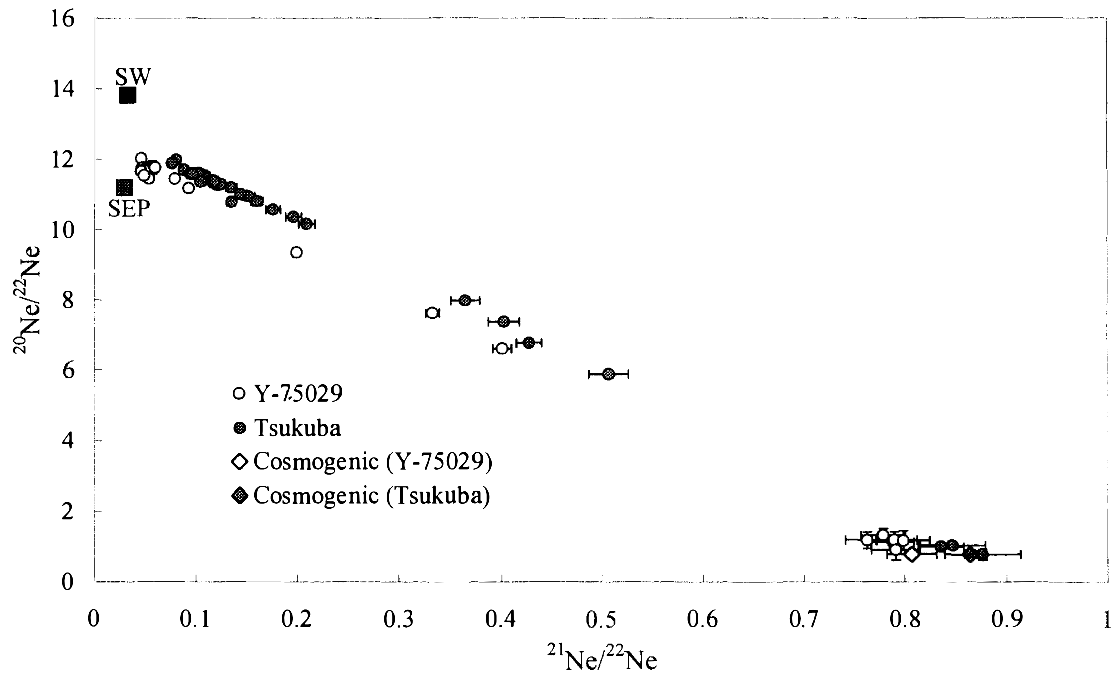

Fig. 1. Ne three-isotope-diagram showing Ne data of many pieces of samples from Y-75029 and Tsukuba H chondrites. For isotopic ratios of Ne-SW and -SEP components, we use values from Benkert et al. (1993), and "cosmogenic" isotopic ratios are obtained in the way shown in Subsection 2.2.

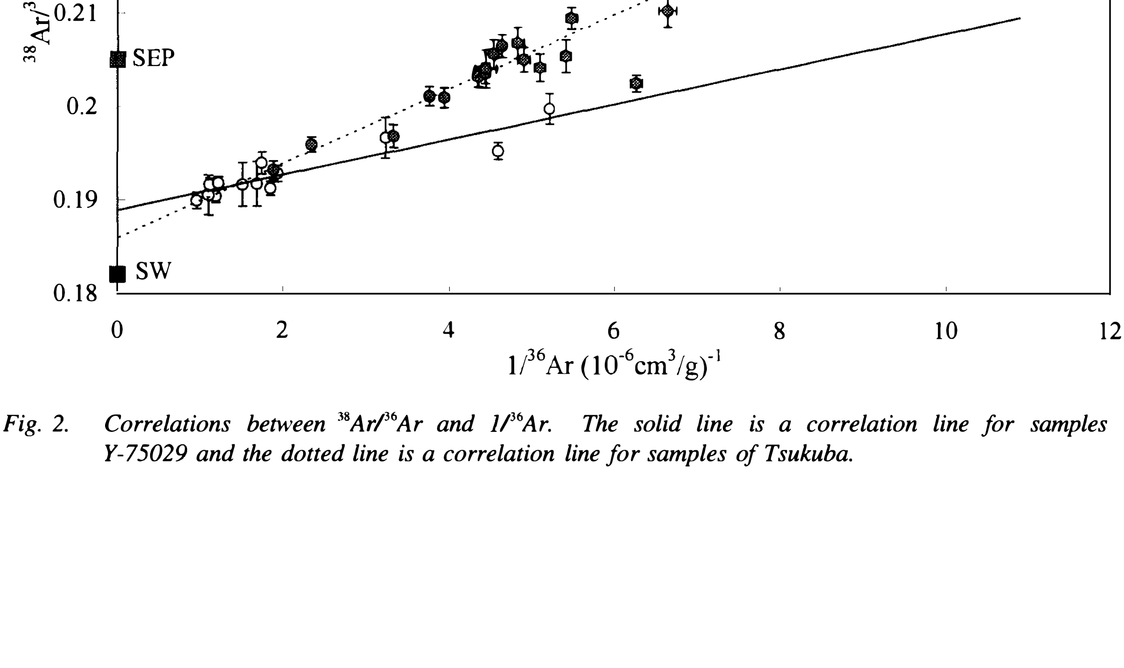

Fig. 2. Correlations between $^{38}Ar/^{36}Ar$ and $1/^{36}Ar$. The solid line is a correlation line for samples of Y-75029 and the dotted line is a correlation line for samples of Tsukuba.

Table 1. He-Ar concentrations and isotopic ratios of Y-75029.

	sample	mass(g)	$^{4}He^{*}$	$^{3}He/^{4}He$	$^{20}Ne^{*}$	$^{20}Ne/^{22}Ne$	$^{21}Ne/^{22}Ne$	$^{40}Ar^{*}$	$^{38}Ar/^{36}Ar$	$^{40}Ar/^{36}Ar$
solar-gas-rich portions	Y1	0.0013	6.51E-04	0.000457 ± 0.000008	1.25E-05	12.02 ± 0.09	0.046 ± 0.001	4.11E-05	0.190 ± 0.001	48.66 ± 1.15
	Y2	0.0016	4.20E-04	0.000562 ± 0.000010	8.60E-06	11.76 ± 0.18	0.057 ± 0.001	3.43E-05	0.190 ± 0.001	33.04 ± 0.76
	Y3	0.0020	4.72E-04	0.000471 ± 0.000006	8.31E-06	11.74 ± 0.04	0.052 ± 0.001	3.01E-05	0.192 ± 0.002	45.41 ± 0.65
	Y4	0.0013	5.50E-04	0.000449 ± 0.000008	1.29E-05	11.75 ± 0.05	0.047 ± 0.001	2.98E-05	0.192 ± 0.001	33.25 ± 0.40
	Y5	0.0021	4.32E-04	0.000503 ± 0.000009	8.64E-06	11.74 ± 0.09	0.052 ± 0.001	2.86E-05	0.192 ± 0.001	34.77 ± 0.27
	Y6	0.0014	1.88E-04	0.000638 ± 0.000038	2.50E-06	11.45 ± 0.06	0.079 ± 0.002	2.75E-05	0.197 ± 0.002	88.89 ± 1.39
	Y14	0.0020	3.64E-04	0.000549 ± 0.000010	8.15E-06	11.70 ± 0.06	0.053 ± 0.001	3.35E-05	0.193 ± 0.001	64.90 ± 0.39
	Y15	0.0021	2.93E-04	0.000508 ± 0.000012	6.75E-06	11.69 ± 0.05	0.049 ± 0.001	1.34E-05	0.191 ± 0.001	24.71 ± 0.39
	Y16	0.0012	4.54E-04	0.000517 ± 0.000005	1.21E-05	11.67 ± 0.04	0.046 ± 0.001	2.59E-05	0.190 ± 0.002	28.54 ± 1.27
	Y17	0.0012	5.27E-04	0.000505 ± 0.000005	1.36E-05	11.66 ± 0.05	0.046 ± 0.001	n.m	n.m	n.m
	Y18	0.0011	3.78E-04	0.000563 ± 0.000005	5.43E-06	11.76 ± 0.07	0.060 ± 0.002	3.49E-05	0.192 ± 0.002	58.78 ± 1.89
	Y19	0.0018	1.28E-04	0.001004 ± 0.000015	2.60E-06	11.17 ± 0.07	0.093 ± 0.002	3.71E-05	0.200 ± 0.002	192.98 ± 1.65
	Y22	0.0174	4.96E-04	0.000481 ± 0.000004	7.17E-06	11.45 ± 0.07	0.054 ± 0.001	4.39E-05	0.195 ± 0.001	200.75 ± 0.55
	Y23	0.0308	6.71E-04	0.000439 ± 0.000004	9.09E-06	11.54 ± 0.05	0.049 ± 0.001	4.51E-05	0.194 ± 0.001	78.61 ± 0.34
solar-gas-poor-portions	Y7	0.0018	1.37E-05	0.005842 ± 0.001534	2.41E-08	1.34 ± 0.19	0.778 ± 0.021	4.24E-05	0.421 ± 0.027	6413.07 ± 665.64
	Y8	0.0023	1.34E-05	0.006053 ± 0.001332	2.07E-08	1.14 ± 0.16	0.788 ± 0.020	3.83E-05	0.433 ± 0.020	5067.03 ± 359.25
	Y9	0.0015	2.60E-05	0.003143 ± 0.000560	2.38E-08	1.21 ± 0.24	0.789 ± 0.022	5.42E-05	0.404 ± 0.030	7523.65 ± 886.39
	Y10	0.0015	2.92E-05	0.002748 ± 0.000449	2.08E-08	1.19 ± 0.28	0.798 ± 0.026	3.36E-05	0.469 ± 0.037	4817.10 ± 579.83
	Y11	0.0020	4.79E-05	0.001891 ± 0.000153	2.70E-07	6.60 ± 0.10	0.401 ± 0.009	4.16E-05	0.254 ± 0.004	1684.49 ± 40.35
	Y12	0.0017	3.91E-05	0.001989 ± 0.000239	2.37E-08	1.21 ± 0.24	0.763 ± 0.022	4.90E-05	0.353 ± 0.018	5902.40 ± 558.76
	Y13	0.0023	1.28E-05	0.006446 ± 0.002629	1.72E-08	0.92 ± 0.29	0.790 ± 0.023	4.07E-05	0.372 ± 0.018	5153.68 ± 441.27
	Y20	0.0371	5.66E-05	0.001772 ± 0.000022	7.85E-07	9.35 ± 0.04	0.200 ± 0.004	n.m	n.m	n.m
	Y21	0.0299	2.62E-05	0.003303 ± 0.000037	3.11E-07	7.61 ± 0.03	0.333 ± 0.007	4.51E-05	0.263 ± 0.004	1924.74 ± 13.91

* Gas concentrations are given in cm^3/g. The errors in gas concentrations are less than 11%, 34% and 12% for ^{4}He, ^{20}Ne and ^{40}Ar, respectively, and include all errors of experiments, standard airs, etc.

n.m.=not measured

Table 2. He-Ar concentrations and isotopic ratios of Tsukuba.

	sample	mass(g)	$^{4}He^{*}$	$^{3}He/^{4}He$	$^{20}Ne^{*}$	$^{20}Ne/^{22}Ne$	$^{21}Ne/^{22}Ne$	$^{40}Ar^{*}$	$^{38}Ar/^{36}Ar$	$^{40}Ar/^{36}Ar$
solar-gas-rich portions	TD1.2	0.0037	7.03E-04	0.000514 ± 0.000012	2.44E-06	10.94 ± 0.09	0.152 ± 0.006	6.69E-05	0.220 ± 0.001	534.47 ± 3.37
	TD1.3	0.0015	4.34E-04	0.000651 ± 0.000015	1.72E-06	10.36 ± 0.09	0.197 ± 0.008	6.93E-05	0.230 ± 0.002	753.79 ± 13.02
	TD2.1	0.0049	9.36E-04	0.000473 ± 0.000020	4.08E-06	11.48 ± 0.10	0.108 ± 0.004	6.75E-05	0.203 ± 0.001	293.85 ± 0.69
	TD2.2	0.0047	7.64E-04	0.000529 ± 0.000018	3.18E-06	11.01 ± 0.07	0.144 ± 0.006	8.07E-05	0.204 ± 0.001	411.50 ± 2.57
	TD2.3	0.0053	1.00E-03	0.000468 ± 0.000023	3.96E-06	11.33 ± 0.07	0.118 ± 0.005	7.36E-05	0.204 ± 0.001	326.31 ± 1.90
	TD2.4.1	0.0036	8.54E-04	0.000466 ± 0.000013	3.10E-06	11.21 ± 0.08	0.135 ± 0.006	7.56E-05	0.205 ± 0.001	370.07 ± 2.09
	TD2.4.2	0.0017	1.03E-03	0.000497 ± 0.000022	3.67E-06	11.40 ± 0.09	0.117 ± 0.005	6.40E-05	0.209 ± 0.001	351.79 ± 2.22
	TD2.5.1	0.0021	6.16E-04	0.000557 ± 0.000014	1.99E-06	10.57 ± 0.07	0.177 ± 0.007	8.27E-05	0.214 ± 0.001	495.33 ± 4.05
	TD2.5.2	0.0015	1.03E-03	0.000451 ± 0.000011	3.70E-06	11.27 ± 0.10	0.122 ± 0.005	8.99E-05	0.207 ± 0.002	434.03 ± 3.69
	TD3.1	0.0035	9.43E-04	0.000475 ± 0.000012	4.29E-06	11.53 ± 0.07	0.109 ± 0.004	6.90E-05	0.201 ± 0.001	272.34 ± 0.65
	TD3.2	0.0056	8.75E-04	0.000458 ± 0.000011	3.47E-06	11.40 ± 0.08	0.115 ± 0.004	1.09E-04	0.206 ± 0.001	506.91 ± 2.10
	TD3.3	0.0096	8.80E-04	0.00046 ± 0.000011	3.68E-06	11.30 ± 0.08	0.124 ± 0.005	7.83E-05	0.206 ± 0.002	355.33 ± 3.66
	TD3.4	0.0046	1.90E-03	0.000369 ± 0.000009	8.73E-06	11.97 ± 0.10	0.081 ± 0.003	7.01E-05	0.193 ± 0.001	132.19 ± 0.50
	TD5	0.0009	6.62E-04	0.000428 ± 0.000004	3.13E-06	11.38 ± 0.11	0.104 ± 0.003	4.22E-05	0.202 ± 0.001	264.48 ± 0.91
	TD6	0.0007	6.13E-04	0.000529 ± 0.000005	2.76E-06	10.81 ± 0.13	0.160 ± 0.006	7.48E-05	0.210 ± 0.002	497.21 ± 3.19
	TD7	0.0013	6.69E-04	0.000527 ± 0.000004	3.11E-06	10.80 ± 0.08	0.135 ± 0.004	7.00E-05	0.220 ± 0.001	506.36 ± 2.07
	TD8	0.0013	1.67E-03	0.000383 ± 0.000003	8.64E-06	11.88 ± 0.09	0.077 ± 0.002	6.36E-05	0.196 ± 0.001	149.00 ± 0.50
	TD9	0.0014	1.34E-03	0.000401 ± 0.000003	6.87E-06	11.69 ± 0.09	0.088 ± 0.002	6.21E-05	0.197 ± 0.001	206.33 ± 0.89
	TD11	0.0012	7.14E-04	0.000454 ± 0.000005	3.59E-06	11.58 ± 0.09	0.095 ± 0.003	5.73E-05	0.205 ± 0.002	310.76 ± 1.12
	TD12	0.0019	5.71E-04	0.000476 ± 0.000005	2.75E-06	11.57 ± 0.10	0.097 ± 0.003	2.98E-05	0.215 ± 0.001	208.08 ± 2.47
	TD13	0.0020	6.86E-04	0.000488 ± 0.000004	3.59E-06	11.37 ± 0.10	0.118 ± 0.003	7.44E-05	0.204 ± 0.002	330.24 ± 4.13
	TL2	0.0119	1.06E-03	0.000436 ± 0.000011	4.44E-06	11.60 ± 0.08	0.103 ± 0.004	7.07E-05	0.201 ± 0.001	266.51 ± 0.87
	TL3	0.0086	3.46E-04	0.000744 ± 0.000018	1.54E-06	10.16 ± 0.07	0.210 ± 0.008	6.65E-05	0.221 ± 0.002	649.35 ± 2.68
solar-gas-poor portions	TD1.1	0.0052	1.80E-04	0.001222 ± 0.000034	5.90E-07	7.37 ± 0.05	0.403 ± 0.015	6.41E-05	0.283 ± 0.003	2087.02 ± 43.07
	TD1.4	0.0014	1.39E-05	0.011509 ± 0.000499	2.77E-08	0.78 ± 0.16	0.876 ± 0.037	n.m.	n.m.	n.m.
	TD3.5	0.0074	2.05E-04	0.001339 ± 0.000032	6.09E-07	7.97 ± 0.06	0.365 ± 0.014	6.73E-05	0.267 ± 0.003	1419.65 ± 15.23
	TD4	0.0019	3.34E-05	0.003544 ± 0.000056	1.62E-07	6.76 ± 0.08	0.428 ± 0.013	6.99E-05	0.220 ± 0.002	370.74 ± 1.83
	TD10	0.0015	2.41E-05	0.007054 ± 0.000101	6.02E-08	1.00 ± 0.05	0.835 ± 0.023	8.65E-05	0.268 ± 0.003	2022.85 ± 21.33
	TL1	0.0125	2.10E-04	0.00198 ± 0.000049	3.38E-07	5.88 ± 0.04	0.507 ± 0.019	6.95E-05	0.300 ± 0.004	2342.53 ± 34.38
	TL4	0.0055	2.24E-05	0.008002 ± 0.000204	4.82E-08	1.05 ± 0.03	0.846 ± 0.032	9.09E-05	0.377 ± 0.011	4830.43 ± 191.18

* Gas concentrations are given in cm^3/g. The errors in gas concentrations are less than 5%, 20% and 5% for ^{4}He, ^{20}Ne and ^{40}Ar, respectively, and include all errors of experiments, standard airs, etc. n.m. = not measured.

Table 3. Y-75029: Concentrations and isotopic ratios of solar ^{20}Ne and concentrations of cosmogenic ^{21}Ne.

	sample	$^{20}Ne_S$*	$(^{20}Ne/^{22}Ne)_S$	$(^{21}Ne/^{22}Ne)_S$	$^{21}Ne_C$*
solar-gas-rich portions	Y1	1.25E-05	12.25	0.0308	1.68E-08
	Y2	8.58E-06	12.14	0.0307	1.99E-08
	Y3	8.29E-06	12.04	0.0306	1.56E-08
	Y4	1.29E-05	11.99	0.0305	1.89E-08
	Y5	8.62E-06	12.05	0.0306	1.61E-08
	Y6	2.49E-06	12.16	0.0307	1.10E-08
	Y14	8.13E-06	12.02	0.0305	1.62E-08
	Y15	6.74E-06	11.96	0.0305	1.13E-08
	Y16	1.21E-05	11.89	0.0304	1.68E-08
	Y17	1.36E-05	11.89	0.0304	1.94E-08
	Y18	5.42E-06	12.19	0.0308	1.40E-08
	Y19	2.59E-06	12.07	0.0306	1.51E-08
	Y22	8.31E-06	11.78	0.0302	1.77E-08
	Y23	1.05E-05	11.81	0.0303	1.76E-08
solar-gas-poor portions	Y7	n.c.	n.c.	n.c.	1.40E-08
	Y8	n.c.	n.c.	n.c.	1.43E-08
	Y9	n.c.	n.c.	n.c.	1.55E-08
	Y10	n.c.	n.c.	n.c.	1.40E-08
	Y11	2.54E-07	11.88	0.0304	1.58E-08
	Y12	n.c.	n.c.	n.c.	1.49E-08
	Y13	n.c.	n.c.	n.c.	1.48E-08
	Y20	7.70E-07	11.73	0.0302	1.48E-08
	Y21	3.11E-07	11.94	0.0304	1.50E-08

* Gas concentrations are given in cm^3/g.
n.c.=not calculated; Isotopic ratios and gas concentrations of solar component are not calculated because of lack of solar Ne.

measured samples are mixtures of solar-Ne and cosmogenic-Ne. The isotopic ratios indicate that solar-Ne are mixtures of SW-Ne and SEP-Ne. The presence of solar gases in the samples of Y-75029 and Tsukuba suggests that solar wind particles were implanted on the surfaces of their parent bodies after the dissipation of nebular gases, because solar winds cannot penetrate the nebular gases (Housen and Wilkening, 1980). Concentrations of $^{20}Ne_S$ and $^{21}Ne_C$ for each sample of Y-75029 and Tsukuba are shown in Tables 3 and 4.

Then, we compare the concentration of $^{20}Ne_S$ with that of $^{21}Ne_C$ (Fig. 3). In Fig. 3, there are fairly good correlations between the concentrations of $^{20}Ne_S$ and $^{21}Ne_C$ in solar-gas-rich portions of Y-75029 and Tsukuba. The interpretation for the correlations is discussed in the Section 4.

4. Interpretation and calculation

4.1. The regolith exposure model

We developed a simple regolith exposure model (Fig. 4) to explain the correlations between $^{20}Ne_S$ and $^{21}Ne_C$ shown in Fig. 3. Figure 4 shows the evolution of the regolith, which proceeds from (a), (b), (c), to (d). The insets show the $^{21}Ne_C$-$^{20}Ne_S$ diagrams for

Table 4. Tsukuba: Concentrations and isotopic ratios of solar ^{20}Ne and concentrations of cosmogenic ^{21}Ne.

	sample	$^{20}Ne_S$*	$(^{20}Ne/^{22}Ne)_S$	$(^{21}Ne/^{22}Ne)_S$	$^{21}Ne_C$*
solar-gas-rich portions	TD1.2	2.41E-06	12.66	0.0313	2.78E-08
	TD1.3	1.69E-06	12.74	0.0315	2.85E-08
	TD2.1	4.06E-06	12.56	0.0312	2.84E-08
	TD2.2	3.15E-06	12.61	0.0313	3.39E-08
	TD2.3	3.93E-06	12.55	0.0312	3.13E-08
	TD2.4.1	3.07E-06	12.68	0.0314	2.96E-08
	TD2.4.2	3.65E-06	12.61	0.0313	2.86E-08
	TD2.5.1	1.96E-06	12.64	0.0313	2.84E-08
	TD2.5.2	3.67E-06	12.54	0.0312	3.08E-08
	TD3.1	4.26E-06	12.64	0.0313	2.99E-08
	TD3.2	3.45E-06	12.59	0.0313	2.64E-08
	TD3.3	3.65E-06	12.61	0.0313	3.12E-08
	TD3.4	8.69E-06	12.67	0.0314	3.72E-08
	TD5	3.11E-06	12.40	0.0310	2.09E-08
	TD6	2.73E-06	12.64	0.0313	3.42E-08
	TD7	3.08E-06	12.22	0.0308	3.11E-08
	TD8	8.61E-06	12.52	0.0312	3.43E-08
	TD9	6.84E-06	12.50	0.0311	3.49E-08
	TD11	3.58E-06	12.47	0.0311	2.05E-08
	TD12	2.74E-06	12.50	0.0312	1.63E-08
	TD13	3.57E-06	12.61	0.0313	2.84E-08
	TL2	4.41E-06	12.62	0.0313	2.86E-08
	TL3	1.52E-06	12.72	0.0314	2.81E-08
solar-gas-poor portions	TD1.1	5.61E-07	12.66	0.0314	3.08E-08
	TD1.4	n.c.	n.c.	n.c.	3.10E-08
	TD3.5	5.84E-07	12.67	0.0314	2.65E-08
	TD4	1.52E-07	12.77	0.0315	9.84E-09
	TD10	n.c.	n.c.	n.c.	5.00E-08
	TL1	3.12E-07	12.67	0.0314	2.84E-08
	TL4	n.c.	n.c.	n.c.	3.89E-08

* Gas concentrations are given in cm^3/g.
n.c.=not calculated; Isotopic ratios and gas concentrations of solar component are not calculated because of lack of solar Ne.

which expected Ne data points of the different portions in regolith are shown.

In stage (a) (Fig. 4 a), the surface of the meteorite parent body is covered with regolith and exposed to SW, SEP, solar cosmic ray (SCR) and GCR. The surface regolith is continuously mixed during cosmic dust bombardment and occasionally by the collisions of meteoroids. For this model, we assume that the material mixed in the regolith, portions "A" (Fig. 4a), has an average chondritic chemical composition, and is exposed to SW, SEP, SCR, and GCR at the depth of 0 to 3 cm (dashed line in Fig. 4a), at which SCR contribution to cosmogenic Ne production is effective. Thus, portions "A" contain increasing amounts of solar and cosmogenic Ne. The portions "A" (Fig. 4a) are plotted as only one discrete point in the $^{21}Ne_C$-$^{20}Ne_S$ diagram (Fig. 4a), because all the

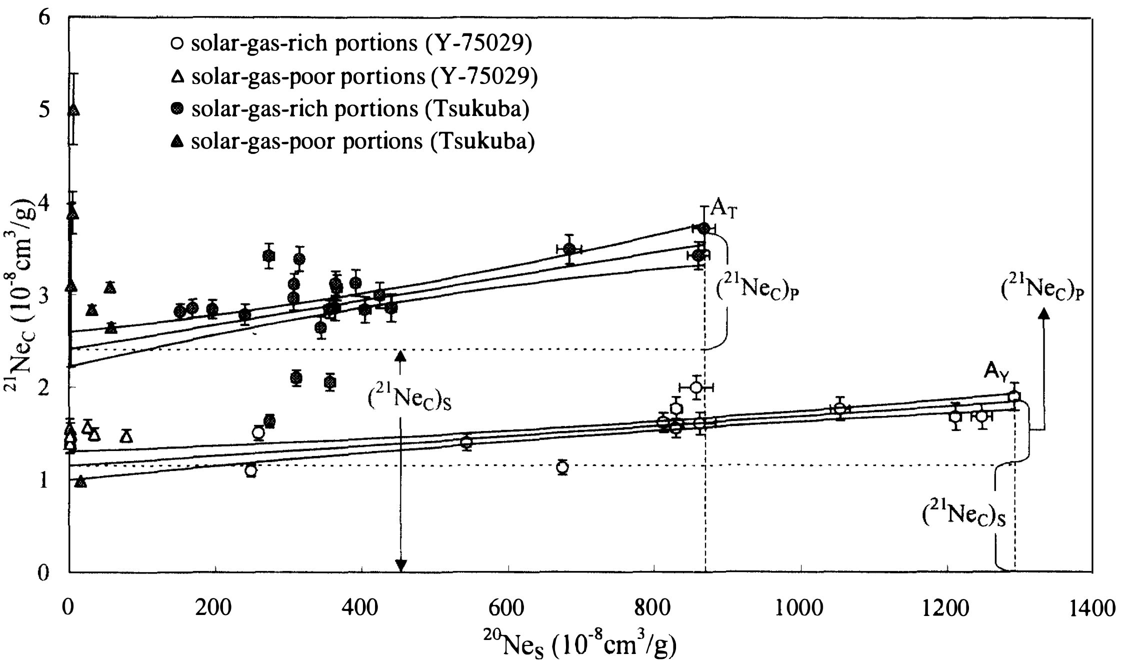

Fig. 3. A relationship between $^{21}Ne_C$ and $^{20}Ne_S$. The solid lines are the correlation lines for solar-gas-rich portions of Y-75029 and Tsukuba. The curved lines are the 1 σ confidence lines for the correlation lines. Points A_Y and A_T are the highest solar gas concentrations of Y-75029 and Tsukuba, respectively, which are correspond to point A in Fig. 4d. The data of Y17 in Table 3 is not plotted because of lack of Ar data. $(^{21}Ne_C)_P$ corresponds to that in Fig. 4d and $(^{21}Ne_C)_S$ corresponds to that in Fig. 4d.

materials were continuously mixed and irradiated similarly. On the other hand, portions "B" (Fig. 4a), having an average chondritic chemical composition, are located at a depth to which even GCR cannot penetrate and thus are plotted on the origin in the Ne diagram (Fig. 4a).

In stage (b) (Fig. 4b), extensive mixing occurs between portions "A" and "B" due to the collisions of a very large meteoroid, and as a result the data points for portions "A+B" are plotted between the points A and B, making a correlation line.

In stage (c) (Fig. 4c), the portions "A+B" are varied deeply by the addition of newly accreted material and shielded from any energetic particles including GCR. For this model no increase is observed in solar and cosmogenic Ne concentrations.

In stage (d) (Fig. 4d), meteoroids including portions "A+B" are ejected from the parent body upon a large-scale impact. The space exposure environment for "A+B" is considered in the following two cases. Case (1): portions "A+B" are located at the interior of the meteoroids. In this case, portions "A+B" are exposed to only GCR, such that only cosmogenic Ne concentration increases in "A+B" during the transit to the earth. Therefore, the correlation line between A and B is shifted up in the Ne diagram (Fig. 4d). Case (2): portions "A+B" are near the surface of the meteoroids. In this case, portions "A+B" are exposed to SW, SEP, SCR, and GCR, but the surface of portions "A+B", where SW and SEP were implanted, are lost during atmospheric entry of the meteoroids. As a result, only cosmogenic Ne concentration increases in portions "A+B" during the

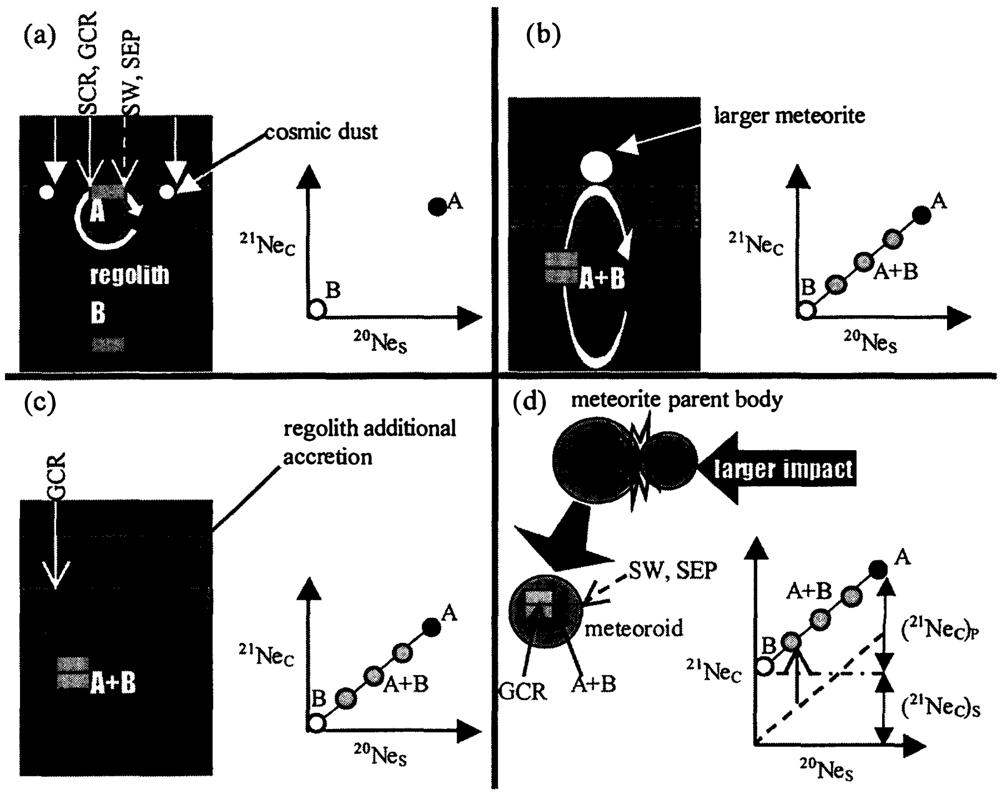

Fig. 4. The regolith exposure model that illustrates evolution from (a), (b), (c) to (d). In each illustration, the left cartoon describes the structure of regolith in the meteorite parent body; the right describes correlations of $^{20}Ne_S$ and $^{21}Ne_C$ in portions "A", "B", and "A+B".

transit to the earth, as in case (1), but the SCR contribution to $^{21}Ne_C$ production must be considered. It is inferred that Y-75029 has experienced case (2), whereas Tsukuba has experienced case (1), which will be discussed in Subsection 4.4.

In this regolith exposure model, parent body exposure with 2π geometry occurred only in stage (a) (Fig. 4a). On the other hand, space exposure, with 4π geometry for GCR and 2π geometry for SCR, took place in stage (d) (Fig. 4d).

4.2. *Interpretation of measured data based on the model*

In this subsection, we look at the correspondence between the Ne diagram from the regolith exposure model (Fig. 4d) and that of the measured data in Fig. 3. The correlation line in Fig. 4d corresponds to that of the measured data in Fig. 3. Portions "A+B" (Fig. 4d) correspond to solar-gas-rich portions (Fig. 3), and portions "B" (Fig. 4d) correspond to solar-gas-poor portions (Fig. 3). Portions "A" (Fig. 4d) are assumed to be the portions for which the Ne data are plotted on points A_Y and A_T for Y-75029 and Tsukuba, respectively (Fig. 3).

The concentration of $^{21}Ne_C$ produced during space exposure corresponds to $(^{21}Ne_C)_S$ in Fig. 4d, and the concentration of $^{21}Ne_C$ produced during parent body exposure corresponds to $(^{21}Ne_C)_P$ in Fig. 4d. $(^{21}Ne_C)_S$ and $(^{21}Ne_C)_P$ in Fig. 4d is equivalent to those in Fig. 3.

Some of the data in Fig. 3 fall far below the correlation lines, whereas others fall above the lines. This may be due to the variation in the chemical composition of each sample, because the cosmogenic Ne production rate varies with chemical composition. The sizes of the samples measured by noble gas analysis are small. Therefore, the heterogeneity of chemical compositions of samples may result in the dispersion of the data from the correlation line in Fig. 3, which will be discussed in Section 5.

4.3. Calculation of the parent body exposure age and the heliocentric distance

The heliocentric distance r_P is the distance of the meteorite parent body from the sun when portions "A" (Fig. 4a) were exposed to SW. To obtain the parent body exposure age T_P and r_P, we prepared the simultaneous equations:

$$T_P=\frac{(^{21}\mathrm{Ne_C})_P}{P_G+P_S/r_P^2}, \tag{4}$$

$$r_P=\sqrt{\frac{(^{36}\mathrm{Ar_S})_L}{T_L}\Bigg/\frac{(^{36}\mathrm{Ar_S})_P}{T_P}}, \tag{5}$$

where suffixes P, L, S and C represent parent body, lunar, solar, and cosmogenic, respectively, and P_G and P_S (at 1 AU) are $^{21}\mathrm{Ne_C}$ production rates by GCR and SCR, in portions "A" (Fig. 4a). On the basis of the regolith exposure model, the shielding depth of the portions "A" (Fig. 4a) is from 0 to 3 cm, corresponding to the linear absorption coefficient from 0 to 10 g/cm^2. The production rate for $^{21}\mathrm{Ne_C}$ during the parent body exposure is the average value for the shielding depth from 0 to 10 g/cm^2, and portions "A" (Fig. 4a) were exposed to both SCR and GCR. Therefore we consider both contributions in $^{21}\mathrm{Ne_C}$ production during the parent body exposure. The equations of P_G and P_S are followings:

$$P_G=518[\mathrm{Mg}]+267[\mathrm{Na}]+242[\mathrm{Al}]+149[\mathrm{Si}]+34.4[\mathrm{Ca}]+3.96[\mathrm{Fe}], \tag{6}$$
$$P_S=869[\mathrm{Mg}]+210[\mathrm{Al}]+69.9[\mathrm{Si}]+0.879[\mathrm{Ca}]+0.0325[\mathrm{Fe}], \tag{7}$$

where the coefficients are the averages of $^{21}\mathrm{Ne_C}$ elemental production rate at the shielding depth from 0 to 10 g/cm^2 (10^{-11} cm^3/g·Ma), which are calculated from the data given by Hohenberg *et al.* (1978), and [X] is the concentration of element X as weight fraction. The concentrations of elements X are adopted from the chemical composition of Y-75029 (Haramura *et al*., 1983) and Tsukuba (Jarosewich, 1990).

P_S is divided by r_P^2 in eq. (4) because SCR flux is in inverse relation to r_P^2. $(^{21}\mathrm{Ne_C})_P$ are shown in Fig. 3 and $(^{36}\mathrm{Ar_S})_P$ are $^{36}\mathrm{Ar_S}$ concentrations of the portions "A" (Fig. 4a),

Table 5. $(^{36}Ar_S)_P$, $(^{21}Ne_C)_P$, and $(^{21}Ne_C)_S$ in Y-75029 and Tsukuba.

meteorite	$(^{36}\mathrm{Ar_S})_P$*	$(^{21}\mathrm{Ne_C})_P$*	$(^{21}\mathrm{Ne_C})_S$*
Y-75029	89.3	$0.74\pm^{0.20}_{0.29}$	1.15±0.16
Tsukuba	52.8	$1.31\pm^{0.24}_{0.58}$	2.41±0.19

* Concentrations are given in 10^{-8}cm^3/g.
These values are deduced as described in section 4.
The errors of $(^{21}\mathrm{Ne_C})_P$ and $(^{21}\mathrm{Ne_C})_S$ are calculated from the 1σ confidence lines in Fig. 3.

Table 6. *($^{36}Ar_S)_L$ abd T_L in lunar meteorites and ($^{36}Ar_S)_L/T_L$.*

meteorite		$(^{36}Ar_S)_L$*	T_L (Ma)	Ref.[a]
QUE93069		34600	420	1
ALHA81005		19500	270	1
EET87521	breccia	1150	15	2
	glass	3840	35	
$(^{36}Ar_S)_L/T_L$#			7.99×10^{-7}	

[a]References: 1: Thalmann and Eugster, (1995); 2: Eugster *et al*., (1996).
* Concentrations are given in $10^{-8}cm^3/g$.
#$(^{36}Ar_S)_L/T_L$ is calculated from $(^{36}Ar_S)_L$ and T_L by applying the least square method.

which correspond to those samples with Ne data falling on points A_Y and A_T (Table 5). Light noble gas data of lunar meteorites, QUE 93069, ALHA 81005 (Thalmann and Eugster, 1995) and breccia and glass of EET 87521 (Eugster *et al*., 1996) are used for the calculation of $(^{36}Ar_S)_L/T_L$ (Table 6).

As found in eq. (5), the concentration of solar noble gases implanted on the portions "A" (Fig. 4a) in the meteorite parent body per unit time is inversely related to r_P^2, because the fluxes of SW and SEP are inversely proportional to r_P^2. The implantation rates of each of the solar gases can be obtained from the solar gas concentrations divided by the exposure duration, which is calculated from the concentration of cosmogenic gases produced in the parent body at a constant rate. Then, r_P can be calculated by comparing the implantation rates of solar gases on the lunar surface (r_P=1 AU), $(^{36}Ar_S)_L/T_L$ with those on the meteorite parent bodies, $(^{36}Ar_S)_P/T_P$.

4.4. *Calculation of the space exposure age*

The space exposure ages T_S of Y-75029 and Tsukuba are obtained by dividing $(^{21}Ne_C)_S$ (Fig. 3 and Table 5) by the production rate, which differs between the two meteorites and suits for the exposure conditions in space of each meteorite.

Y-75029: As pointed out in Subsection 4.1, Y-75029 may have experienced the space exposure in case (2), because Y-75029 (84 g), paired with a much larger meteorite Y-75028 (6100 g) (Yanai and Kojima, 1987), is likely to have been located near the surface of Y-75028 in space. Besides, the $(^{21}Ne/^{22}Ne)_C$ of Y-75029 is very low and cannot be explained by only a GCR contribution. Assuming that both Y-75029 and Y-75028 were spheres, with radii about 2 cm and 8 cm, respectively, the center of Y-75029 would have been located at about 2 cm from the surface of Y-75028. According to this presumption, $^{21}Ne_C$ production rate of Y-75029 in the space exposure (P_Y; unit of 10^{-10} $cm^3/g\cdot Ma$) can be obtained by the following equation:

$$P_Y=85.3[Na]+165[Mg]+81.9[Al]+45.2[Si]+8.98[Ca]+1.90[Fe]+1.79[Ni], \quad (8)$$

where [X] is the concentration of element X as weight fraction. The coefficients in the equation are the sums of $^{21}Ne_C$ elemental production rates by GCR and those by SCR at 1 AU. $^{21}Ne_C$ elemental production rates by GCR are modeled as a spherical meteoroid with 10 cm in diameter and a shielding depth d/R (depth/radius) of 0.2 to 0.3 (Leya *et al*., 2000). On the other hand, $^{21}Ne_C$ elemental production rates by SCR are the data with shielding depth of 5 g/cm^2 (*cf.* Hohenberg *et al.*, 1978) and at 1 AU, at which the SCR contribution in the most effective. However, the meteoroids were exposed to the sun during their transit from the parent body to the earth. Thus, the SCR production rate at 1 AU is overestimated and T_S is underestimated. From this assumption, T_S of Y-75029 is the lower limit.

Tsukuba: As shown in Subsection 4.1, Tsukuba may have experienced the space exposure in case (1), because $(^{21}Ne/^{22}Ne)_C$ of Tsukuba can be explained by only GCR contribution. But we cannot estimate where our Tsukuba sample was located in the meteoroid, because the Tsukuba meteorite fell as a meteorite shower of 23 fragments (Yoneda *et al.*, 1996). Therefore, the $^{21}Ne_C$ production rate of Tsukuba in the space exposure (P_T; unit of 10^{-10}cm^3/g·Ma) was obtained, assuming an average shielding, from the following equation given by Schultz and Freundel (1985):

$$P_T=163[Mg]+60[Al]+32[Si]+22[S]+7[Ca]+2.1[Fe+Ni], \tag{9}$$

where [X] is the concentration of element X as weight fraction.

5. Results of calculation and discussion

Table 7 shows the calculated T_P, r_P, and T_S for Y-75029 and Tsukuba. T_P is the lower limit, because "true" portions "A" (Fig. 4d) might contain larger amounts of solar and cosmogenic noble gases than the samples represented by points A_Y and A_T in Fig. 3. T_S for Y-75029 and Tsukuba are around the main peak at 7 Ma in the $^{21}Ne_C$ exposure age distribution for H chondrites (Schultz *et al.*, 1991). We discussed the lower limit of T_S of Y-75029 in Section 4, but did not refer to the upper limit. For this, we use the $^{21}Ne_C$ elemental production rate by SCR at 2.2 AU (r_P of Y-75029). The obtained T_S of Y-75029 is 5.8 Ma, which is the upper limit, because the SCR production rate is underestimated. Then, we compared obtained r_P for Y-75029 and Tsukuba with the asteroid distribution in the present solar system. The parent bodies of H chondrites are thought to be S-type asteroids (Chapman, 1996; Dukes *et al.*, 1999; Sasaki *et al.*, 2001). Figure 5 shows the asteroid distribution in the present solar system (Gradie and Tedesco, 1982). As this figure shows, the orbits of S-type asteroids range from 2 to 3.5 AU. On the other hand, the obtained heliocentric distances of Y-75029 and Tsukuba indicate that the locations of the parent bodies in the past when some parts of the meteorites were

Table 7. Results of calculations.

meteorite	r_P (AU)	T_P (Ma)	T_S (Ma)
Y-75029	$2.2\pm^{0.3}_{0.6}$	$5.5\pm^{1.8}_{2.7}$	5.2-5.8
Tsukuba	$4.2\pm^{0.4}_{1.2}$	$11.8\pm^{2.3}_{5.6}$	8.1±0.6

The errors of r_P and T_P are calculated using the errors of $(^{21}Ne_C)_P$ and equations (4) and (5). The error of T_s of Tsukuba is calculated using the error of $(^{21}Ne_C)_S$ and equation (9). The lower and upper limits of T_S of Y-75029 are discussed in sections 4 and 5.

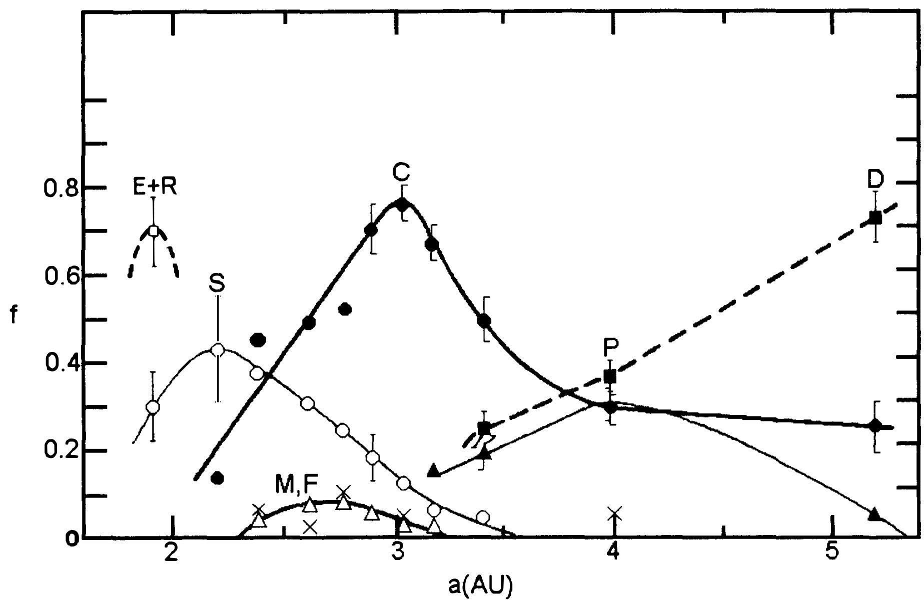

Fig. 5. Asteroid distribution in the present solar system (Gradie and Tedesco, 1982). The transverse represents the heliocentric distance and the ordinate represents the fractions of each asteroid type.

exposed to the sun. The heliocentric distance of Y-75029 is in a good agreement with current S-type asteroid distribution. On the other hand, the heliocentric distance of Tsukuba is in the upper tail of S-type asteroid distribution. It is therefore inferred that the heliocentric distance of S-type asteroids are relatively constant from a certain period in the past to present.

As pointed out in Subsection 4.2, the deviation of the Ne data from the correlation lines are observed in Fig. 3. Figures 6a and b show the $^{21}Ne_C$ production rates for the bulk chemical compositions of Y-75029 ("chondritic" in Fig. 6a) and Tsukuba ("chondritic" in Fig. 6b) and those for the major constituent minerals in H chondrites. As this figure shows, $^{21}Ne_C$ production rate for forsterite (Mg_2SiO_4) is twice as large as that of the chondritic sample in both the cases for parent body exposure and space exposure. The $^{21}Ne_C$ production rate for metallic iron is one order of magnitude smaller than that of the chondritic sample for both cases for parent body and space exposure. Thus, $^{21}Ne_C$ production rates might differ greatly between small pieces of meteorites with different compositions, which would result in the dispersion of the data from the correlation line representing correlations between samples with chondritic composition. It is inferred that some data points lying far above the correlation lines are Mg-rich, whereas others falling below the lines are Mg-poor (Fig. 3).

Next, we discuss the SCR contribution to T_P. Wieler *et al.* (1989) calculated the parent body exposure age using only P_G, because P_G is much larger than P_S/r_P^2. In this study, based on the regolith exposure model (Fig. 4), the SCR contributions to T_P are calculated to be 21.4% and 6.9% for Y-75029 and Tsukuba, respectively (see "chondritic column" in Figs. 6a, b). Thus the SCR contribution to T_P is not significant, but cannot be ignored in case of shielding depths from 0 to 10 g/cm^2.

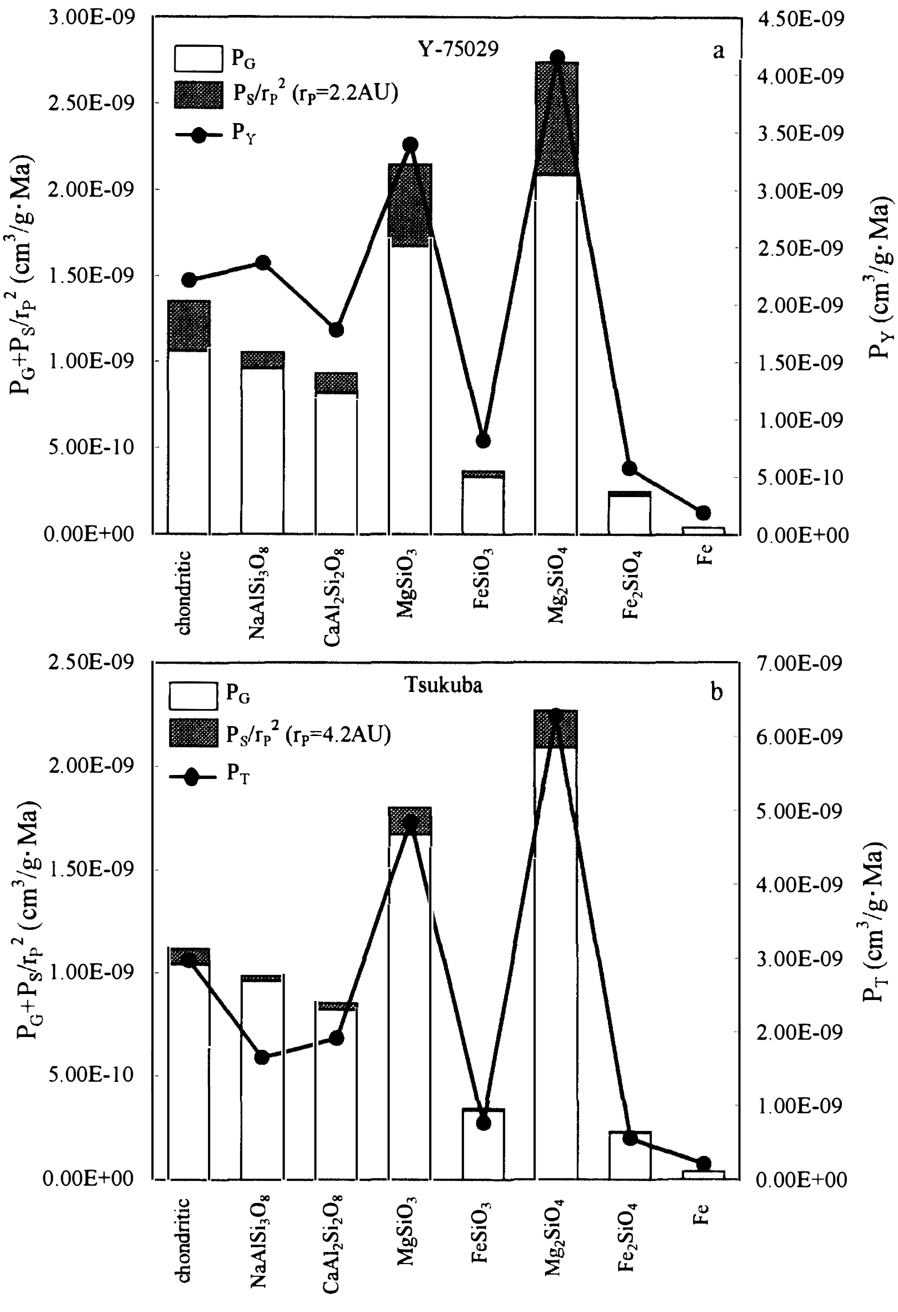

Fig. 6. *$^{21}Ne_C$ production rates for a piece of samples having bulk composition ("chondritic") and those for major constituent minerals in Y-75029 (a) and Tsukuba (b). Units on the left ordinate are for the $^{21}Ne_C$ production rate in the parent body exposure, which are calculated from eqs. (6) and (7), whereas those on the right ordinate are for the $^{21}Ne_C$ production rate in the space exposure, which are calculated from eqs. (8) and (9).*

6. Conclusions

The concentrations and isotopic ratios of light noble gases in H chondrites Y-75029 and Tsukuba were determined in order to calculate the parent body exposure ages, heliocentric distances of the parent body, and the space exposure ages. The parent body exposure ages are more than 5.5 Ma and 11.8 Ma for Y-75029 and Tsukuba, respectively. The heliocentric distances are $2.2\pm^{0.3}_{0.6}$ AU and $4.2\pm^{0.4}_{1.2}$ AU for Y-75029 and Tsukuba, respectively. The space exposure age of Y-75029 is 5.2–5.8 Ma, whereas that of Tsukuba is 8.1 ± 0.6 Ma.

Acknowledgments

We thank the National Institute of Polar Research for providing meteorite samples, Dr. Okazaki for discussion, and Mr. Shimada for technical support in the EPMA analysis. We thank two anonymous reviewers for intensive and constructive reviews. This work has been supported by the Grant-in-aid of the Japan Ministry of Education, Science and Culture to TN (13740318).

References

Anders, E. (1975): Do stony meteorites come from comets? Icarus, **24**, 363–371.

Benkert, J.-P., Baur, H., Signer, P. and Wieler, R. (1993): He, Ne and Ar from the solar wind and solar energetic particles in lunar ilmenites and pyroxenes. J. Geophys. Res., **98**, 13147–13162.

Chapman, C.R. (1996): S-type asteroids, ordinary chondrites, and space weathering: The evidence from Galileo's fly-bys of Gaspra and Ida. Meteorit. Planet. Sci., **31**, 699–725.

Dukes, C. A., Baragiola, R. A. and McFadden, L. A. (1999): Surface modification of olivine by H^+ and He^+ bombardment. J. Geophys. Res., **104**, 1865–1872.

Eugster, O. (1988): Cosmic-ray production rates for ^{3}He, ^{21}Ne, ^{38}Ar, ^{83}Kr and ^{126}Xe in chondrites based on ^{81}Kr-Kr exposure ages. Geochim. Cosmochim. Acta, **52**, 1649–1662.

Eugster, O., Thalmann, Ch., Albrecht, A., Herzog, G.F., Delaney, J.S., Klein, J. and Middleton, R. (1996): Exposure history of glass and breccia phases of lunar meteorite EET 87521. Meteorit. Planet. Sci., **31**, 299–304.

Gradie, J. and Tedesco, E. (1982): Compositional structure of the asteroid belt. Science, **216**, 1405–1407.

Grossman, J.N. (1996): The meteoritical bulletin, No. 80, 1996 July. Meteorit. Planet. Sci., **31**, A175–A180.

Haramura, H., Kushiro, I. and Yanai, K. (1983): Chemical compositions of Antarctic meteorites I. Mem. Natl Inst. Polar Res., Spec. Issue, **30**, 109–121.

Hohenberg, C.M., Marti, K., Podosek, F.A., Reedy, R.C. and Shirck, J.R. (1978): Comparisons between observed and predicted cosmogenic noble gases in lunar samples. Proc. Lunar Planet. Sci. Conf., 9th, 2311–2344.

Housen, K.R. and Wilkening, L.L. (1980): Solar-ion penetration in the early solar nebula. Proc. Lunar Planet. Sci. Conf., 11th, 1251–1269.

Housen, K.R., Wilkening, L.L., Chapman, C.R. and Greenberg, R. (1979): Asteroidal regoliths. Icarus, **39**, 317–351.

Jarosewich, E. (1990): Chemical analyses of meteorites: A compilation of stony and iron meteorite analyses. Meteoritics, **25**, 323–337.

Keil, K. (1982): Composition and origin of chondritic breccias. LPI Tech. Rep., **82-02**, 65–83.

Keller, L.P. and McKay, D.S. (1997): The nature and origin of rims on lunar soil grains. Geochim. Cosmochim. Acta, **61**, 2331–2341.

Leya, I., Lange, H.-J., Neumann, S., Wieler, R. and Michel, R. (2000): The production of cosmogenic nuclides in stony meteoroids by galactic cosmic-ray particles. Meteorit. Planet. Sci., **35**, 259–286.

Nakamura, T. and Takaoka, N. (2000): Solar-wind derived light noble gases in micrometeorites collected at the Dome Fuji Station: Characterization by stepped pyrolysis. Antarct. Meteorite Res., **13**, 311–321.

Okazaki, R., Takaoka, N., Nakamura, T. and Nagao, K. (1998): Exposure history of the H-chondrite Tsukuba (abstract). Antarctic Meteorites XXIII. Tokyo, Natl Inst. Polar Res., 117–119.

Pellas, P. (1972): Irradiation history of grain aggregates in ordinary chondrites, possible clues to the advanced stages of accretion. From Plasma to Planet, ed. by A. Elvius. New York, Wiley, 65–92.

Rajan, R.S. (1974): On the irradiation history and origin of gas-rich meteorites. Geochim. Cosmochim. Acta, **38**, 777–788.

Sasaki, S., Nakamura, K., Hamabe, Y., Kurahashi, E. and Hiroi, T. (2001): Production of iron nanoparticles by laser irradiation in a simulation of lunar-like space weathering. Nature, **410**, 555–557.

Schultz, L. and Freundel, M. (1985): On the production rate of ^{21}Ne in ordinary chondrites. Isotopic Ratios in the Solar System, ed. by Centre National d'Etudes Spatiales. Toulouse, Cepadues-Editions, 27–33.

Schultz, L., Signer, P., Lorin, J.C. and Pellas, P. (1972): Complex irradiation history of the Weston chondrite. Earth Planet. Sci. Lett., **15**, 403–410.

Schultz, L., Weber, H.W. and Begemann, F. (1991): Noble gases in H-chondrites and potential differences between Antarctic and non-Antarctic meteorites. Geochim. Cosmochim. Acta, **55**, 59–66.

Signer, P. (1964): Primordial rare gases in meteorites. The Origin and Evolution of Atmospheres and Oceans. New York, J. Wiley, 183–190.

Suess, H.E., Wänke, H. and Wlotzka, F. (1964): On the origin of gas rich meteorites. Geochim. Cosmochim. Acta, **28**, 209–233.

Takaoka, N., Saito, K., Ohba, Y. and Nagao, K. (1981): Rare gas studies of twenty-four antarctic chondrites. Mem. Natl Inst. Polar Res., Spec. Issue, **20**, 264–275.

Thalmann, Ch. and Eugster, O. (1995): Lunar meteorite Queen Alexandra Range 93069: History derived from cosmic-ray-produced and trapped noble gases. Meteoritics, **30**, 585–586.

Van Schmus, W.R. and Wood, J.A. (1967): A chemical-petrologic classification for the chondritic meteorites. Geochim. Cosmochim. Acta, **31**, 747–765.

Wänke, H. (1965): Der Sonnenwind als Quelle der Uredelgase in steinmeteoriten. Z. Naturforsch., **20a**, 946–949.

Wieler, R., Baur, H., Pedroni, A., Signer, P. and Pellas, P. (1989): Exposure history of the regolithic chondrite Fayetteville: I. Solar-gas-rich matrix. Geochim. Cosmochim. Acta, **53**, 1441–1448.

Wilkening, L.L. (1971): Particle track studies and the origin of gas-rich meteorites. Nininger Meteorite Award Paper, Arizona State University, Tempe.

Yanai, K. and Kojima, H. comp. (1987): Catalog of Japanese collections of the Antarctic meteorites, collected from December 1969 to January 1987. Photographic Catalog of the Antarctic Meteorites. Tokyo, Natl Inst. Polar Res., 223–298.

Yoneda, S., Shima, M., Komura, K., Nagao, K., Okada, A., Kita, N.T., Togashi, S., Okuyama, Y. and Bunno, M. (1996): A new meteorite shower, Tsukuba: Detection of ^{24}Na and the exposure history. Meteorit. Planet. Sci., **31**, A157–A158.

(Received September 26, 2001; Revised manuscript accepted January 7, 2002)